Available online at www.sciencedirect.com
ScienceDirect
Polymer 48 (2007) 1096–1104
polymer
www.elsevier.com/locate/polymer

Morphology and mechanical properties of Nylon 6/MWNT nanofibers

Moncy V. Jose [a], Brian W. Steinert [b,c,1], Vinoy Thomas [a,2], Derrick R. Dean [a,*], Mohamed A. Abdalla [a], Gary Price [d], Gregg M. Janowski [a]

[a] *Department of Materials Science and Engineering, University of Alabama at Birmingham (UAB), 1530 3rd Avenue, South, Birmingham, AL 35294-4461, USA*
[b] *Department of Physics, Rhodes College, Memphis, TN 38112, USA*
[c] *Department of Biology, Rhodes College, Memphis, TN 38112, USA*
[d] *University of Dayton Research Institute, Dayton, OH 45469, USA*

Received 19 June 2006; received in revised form 8 December 2006; accepted 11 December 2006
Available online 20 December 2006

Abstract

Aligned nanofibrous nanocomposites of Nylon 6 and surface-modified multiwalled carbon nanotubes (MWNTs) were successfully synthesized via electrospinning, using a rotating mandrel. Scanning electron microscopy (SEM), differential scanning calorimetry (DSC), X-ray diffraction (XRD), transmission electron microscopy (TEM) and dynamic mechanical analysis (DMA) were done to characterize the morphology and properties of the nanofibrous mats. DSC and XRD observations suggested the presence of MWNTs and the high speed take-up facilitated the transformation of Nylon 6 from γ phase crystals to a mixture of α and γ phase crystals. TEM and WAXD were used to characterize the nanotube and molecular orientations, respectively. The storage modulus of the fibers increased significantly although the concentration of MWNTs was relatively low (0.1 and 1.0 wt%). Thus the combination of carbon nanotubes and nanoscale processing results in structural and mechanical enhancements of Nylon 6.

Keywords: Electrospinning; Nylon 6; Modified MWNT

1. Introduction

Nanocomposites based on carbon nanotubes (CNTs) have received a tremendous amount of attention during the past five years. Individually, CNTs can achieve very high aspect ratios because their diameters are in the range of a few nanometers with lengths of several hundred nanometers. Additionally, CNTs are reported to have an extremely high elastic modulus, ~1 TPa which is comparable to that of diamond (1.2 TPa). The strength of CNTs is 10–100 times that of the strongest steel but at a fraction of the weight [1–4]. CNTs exhibit a range of electrical conductivity, from metallic to moderate band gap semiconductors depending on their structure [5]. Potential applications of polymer/CNT nanocomposites include aerospace and automotive materials (high temperature, light weight), optical switches, EMI shielding, photovoltaic devices, packaging (films, containers), adhesives and coatings. However, the foundations for harnessing the wealth of physics present within nanotube structures hinge on an ability to optimize the dispersibility and orientation of nanotubes in host materials. While a number of studies have reported on polymer/CNT nanocomposites in which certain properties have been enhanced, the largest property enhancements will be realized for nanocomposites with controlled spatial distribution of the CNTs and controlled polymer/CNT interfaces. In particular, nanotube alignment is important, because in addition to mechanical properties, functional properties, such as electrical,

* Corresponding author. Tel.: +1 205 975 4666; fax: +1 205 934 8485.
E-mail address: deand@uab.edu (D.R. Dean).
[1] Current address: Department of Materials Science and Engineering, University of Alabama at Birmingham (UAB), 1530 3rd Avenue, South, Birmingham, AL 35294-4461, USA.
[2] Current address: National Institute of Standards and Technology, Materials Science and Engineering Laboratory, 100 Bureau, Gaithersburg, MD 20899-8500, USA.

0032-3861/$ - see front matter © 2006 Elsevier Ltd. All rights reserved.
doi:10.1016/j.polymer.2006.12.023

magnetic and optical properties, of polymer/CNT nanocomposites are linked directly to the alignment of carbon nanotubes in the matrix.

Several methods have been explored for preparing aligned CNTs in a polymer matrix, including ex situ methods [6–8], and a range of force field methods such as mechanical shear [9,10], magnetic [11,12] and electric fields [13]. Nanotube alignment induced by electric fields is of relevance to our study. Recently, electrospinning has emerged as an ideal route for the production of aligned nanotube based nanofibrous nanocomposites [14–18]. This technique involves applying a high voltage to a polymer solution in a syringe and when the voltage applied reaches a certain threshold limit, the polymer solution overcomes surface tension and ejects a fine jet of liquid from the tip of the needle and deposits on the collector. The polymer jet formed undergoes a uniaxial stretching (or elongation) by whipping instability, which reduces the fiber dimension from micron size (inner diameter of needle) to nanometer size, before depositing on the collector [19,20]. This resulting nanofiber has several important characteristics such as very large surface area to volume ratio (10^3 times that of a micro-fiber), and flexibility in surface functionalities [21].

A number of polymer/CNT systems (both single and multiwalled nanotubes) have been electrospun, including polyethylene oxide (PEO) [17,22], poly(methylmethacrylate) (PMMA) [23,24], poly(acrylonitrile) (PAN) [25,26], copolymers of poly(lactic acid) (PLA) and PAN [27], and thermoplastic polyurethanes [28]. Dror et al. [22] used electrospinning to fabricate nanofibers of poly(ethylene oxide) (PEO) with MWNTs. The MWNTs were in the nanofibers as individual elements, mostly aligned along the fiber axis although at some places they were seen to be dispersed at various angles of the fiber axis. Continuous carbon nanotube filled nanofiber yarns were synthesized by Ko et al. [27]. The aligned nanotube polymer nanofibers (copolymer of PLA and PAN) showed significant improvement in mechanical properties as well as an increase in the melting point. Salalha et al. [17] synthesized composite nanofibers of poly(ethylene oxide) and single walled carbon nanotubes. Well-dispersed and separated nanotubes were embedded in a straight and aligned form. Sung et al. [23] synthesized a nanofibrous membrane of poly(methylmethacrylate) and functionalized MWNT. The nanotubes were embedded and well aligned within the individual fibers. Excellent wrapping of the polymer chains around the MWNT was considered as a reason for reduction in electrical conductivity of the nanocomposite. Nanotube reinforced polyurethane and polystyrene nanofibers were synthesized by Sen et al. [28]. Ester functionalized single walled nanotubes were used for the synthesis of nanofiber nanocomposite. The functionalization of the SWNTs had a significant effect on the mechanical properties of the composite. The tensile strength of Ester–SWNT–PU membranes was enhanced by 104% as compared to electrospun pure polyurethane membranes, while an increase of only 46% was achieved by incorporating as unmodified-SWNT in the polyurethane matrix. Ge et al. [25] synthesized highly oriented, large area continuous composite nanofiber sheets made from surface-oxidized MWNTs and poly(acrylonitrile). A threefold improvement in tensile modulus was observed with the addition of 20% by weight of nanotubes.

In the present study, Nylon 6 is used for the synthesis of aligned MWNT based nanofibrous nanocomposites via electrospinning. Nylon is one of the most widely used commercial polymer fibers with a wide range of applications. A variety of techniques have been used to synthesize Nylon 6 fibers including melt spinning, wet spinning and dry spinning and electrospinning [29–35]. The fibers synthesized are composed of varying amounts of the two common crystalline forms of Nylon 6, the thermodynamically stable α form and the less stable γ form. The crystalline form obtained depends on the collecting speed, thermal treatment and thermo-mechanical history. A high speed rotating collector was used to collect aligned surface-modified MWNTs in the polymer matrix. The evolution of the crystal structure during processing was investigated using DSC, XRD and TEM. Mechanical properties of the fibers are correlated with the processing and morphology.

2. Experimental

2.1. Polymer solution preparation

Nylon 6 (RTP Company, USA) and 1,1,1,3,3,3-hexafluor-2-propanol (HFP) from Fluka®, Sigma-Aldrich, USA were used as received. Multiwalled carbon nanotubes (MWNTs), commercially obtained from MER Corp. (USA) were produced by the arc discharge method and had a purity of 95%. The MWNT obtained had a diameter in the range of 50–100 nm. The surfaces of the MWNTs were modified by attaching carboxylic acid functional groups. This was done by first treating with sulfuric acid/nitric acid (3:1 v/v) followed by sonicating in a bath for 3 h at ambient temperature. The mixture was then purified by washing with distilled water (1:5 by volume) until the complete removal of acid and was then filtered [36]. Two different MWNT weight percentages, 0.1 and 1% were used for the fiber synthesis. A two-step method was used for the dispersion of the MWNTs in the polymer solution. Initially the nanotubes (0.1 and 1.0% by weight) were dispersed in HFP in a 25 mL vial and sonicated for 1 h to disrupt possible agglomerates. The volume of water in the bath was enough to prevent any rise in temperature. In the second step, the proper weight of Nylon 6 pellets was added to the above-mentioned solution to obtain the 10% by weight of Nylon 6/MWNT solution.

2.2. Electrospinning process

The electrospinning apparatus was composed of several components: a high-voltage supply (Gamma High Voltage Research, M826, USA), a syringe with a stainless steel needle (21½ gauge), a syringe pump (KD Scientific Apparatus, USA), and a stainless steel collecting drum (diameter 2.5 cm). Aligned fibers were fabricated at three different collector rotating speeds, 3000, 4500 and 6000 rpm corresponding to linear velocities of 4, 6 and 8 m/s. A voltage of 15 kV was

applied to the needle and the syringe pump was set at a flow rate of 5 mL/h. The collecting drum was maintained at a distance of 15 cm from the tip of the needle and the electrospinning process was conducted at ambient temperature.

2.3. Structural and morphological characterizations

2.3.1. Scanning electron microscopy

A scanning electron microscope (Philips SEM 515, Holland) was used to characterize the morphology of the electrospun nanofibers. The samples were sputter coated with gold and examined at an accelerating voltage of 10 kV.

2.3.2. Differential scanning calorimetry

A differential scanning calorimeter (TA Instruments DSC Q100) was used to study the melting behavior of the nanofibers. The sample was ramped at 10 °C/min from room temperature to 250 °C under a nitrogen atmosphere.

2.3.3. X-ray diffractometry

X-ray diffraction patterns were obtained using a Siemens D500 diffractometer. A voltage of 40 kV and a current of 30 mA using a Cu Kα radiation ($\lambda = 1.5418$), 0.02° 2-θ step and a dwell time of 5 s per step were used. A Rigaku RU200 rotating anode generator equipped with a Stratton camera was used to acquire two-dimensional Wide Angle X-ray Diffraction (WAXD) patterns. Nickel filtered Cu Kα radiation was used at an accelerating voltage of 50 kV/170 mA. The data were collected on phosphor image plates and digitized using a Molecular Dynamics scanner.

2.3.4. Mechanical characterization

The storage modulus of the non-woven nanofibrous mats obtained was measured using a Dynamic Mechanical Analyzer equipped with a tensile fixture (TA Instruments DMA 2980). The tensile force was applied parallel to the orientation direction. A frequency sweep from 0.1 to 100 Hz using an amplitude of 15 μm and a preload force of 0.01 N were used to get the viscoelastic response at room temperature.

3. Results and discussion

3.1. Morphological characterization

The morphology of the electrospun fiber is greatly influenced by the polymer solution properties (viscosity, surface tension, etc.). The optimization of this parameter was obtained by varying the concentration of the polymer solution. The optimized solution was then spun on a static collector and the morphology of the non-woven was studied using SEM. An SEM image of pure Nylon 6 spun onto a static collector (Fig. 1) shows relatively smooth, defect-free fibers. Also the fibers obtained had cylindrical morphology and no fiber bundles, indicating that the tip-to-collector distance was adequate for proper evaporation of the solvent. The diameters of the fibers obtained were within the range of 600 nm–1.5 μm.

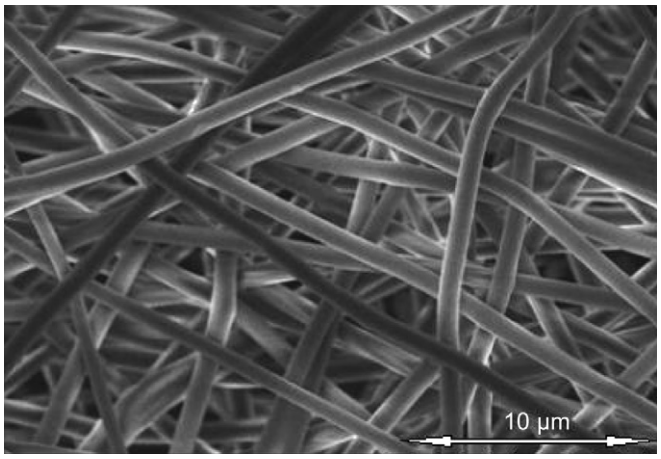

Fig. 1. SEM of non-woven, randomly oriented Nylon 6 fiber mat with uniform diameters.

Aligned electrospun fibers of pure Nylon 6, collected at varying collector speeds are shown in Fig. 2. At 4500 rpm the fiber diameter decreased to a range of 500 nm–900 nm, which is much lower than the diameters in the randomly oriented fiber mat, suggesting that further stretching of the fibers is obtained with rotation of the collector system. This stretching effect as well as the whipping elongation contributes to the alignment of the nanotubes in the polymer fiber. Fig. 3 shows SEM images of nanocomposite fibers with 0.1% by weight of MWNT. These fibers have significantly smaller diameters than the neat Nylon 6 fibers, ranging from 250 nm to 750 nm. A similar trend in the morphology was observed on Nylon 6/1.0 wt% MWNT nanocomposite fibers.

3.2. Melting, crystallization and orientation behaviors

XRD and DSC studies were used to study the melting and crystallization behaviors of both the neat Nylon 6 and the Nylon 6/MWNT nanocomposite nanofibers. Fig. 4 shows XRD scans acquired in reflectance mode for the neat resin at different collector speeds. A diffraction peak at 2θ angle of 22°, characteristic of γ crystals, was observed for the neat Nylon 6 nanofiber specimen collected at 3000 rpm [37]. As the take-up speed increases, in addition to the γ phase, two distinct peaks at 2θ angles of 20° and 24° (d-spacing of 4.43 Å and 3.7 Å, respectively), characteristic of the α phase also appear, suggesting that a mixture of the α and γ phases is now present. The γ phase remains the dominant phase, however. The α phase is known to be the thermodynamically stable phase, and consists of sheets of hydrogen-bonded chains, packed in an anti-parallel manner. The γ phase is the least stable phase, and arises from random hydrogen bonding between parallel chains [37]. Clark has shown, for several configurationally directional polymers, including Nylon 6 that polymorphism must occur during fiber formation from the melt, since only a portion of folded chains is unfolded [38]. In our case, the rapid solvent evaporation during spinning leads to the less ordered γ phase, and the increased rotation speed of the collector helps to partially transform the structure to α phase.

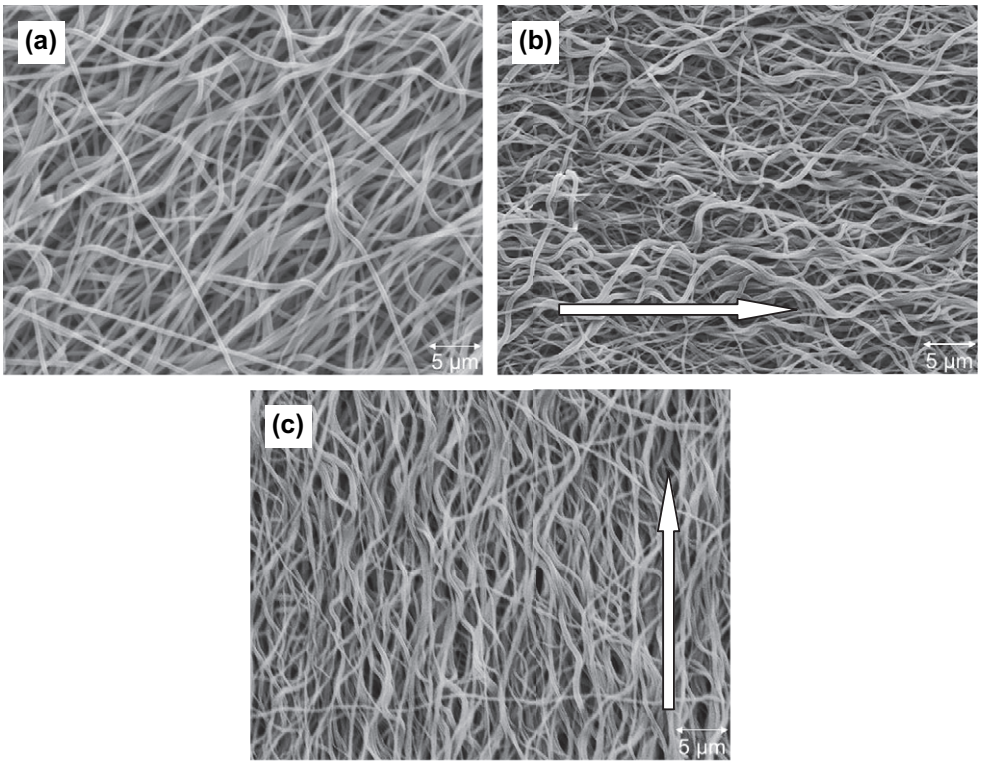

Fig. 2. SEM image of neat Nylon 6 fibers collected at (a) 3000, (b) 4500 and (c) 6000 rpm. Arrows denote alignment direction.

These findings are also consistent with those reported by other researchers [33,34]. Fig. 5 shows the effect of carbon nanotube loadings on the Nylon 6 structure, for a collector speed of 3000 rpm. As the nanotube loadings increase, the structure transforms from the single γ phase for the neat Nylon 6, to a mixture of γ and the more stable α phases. Fong et al. [35] have shown that cast films of Nylon 6 showed only the presence of α crystals while electrospun fibers showed γ

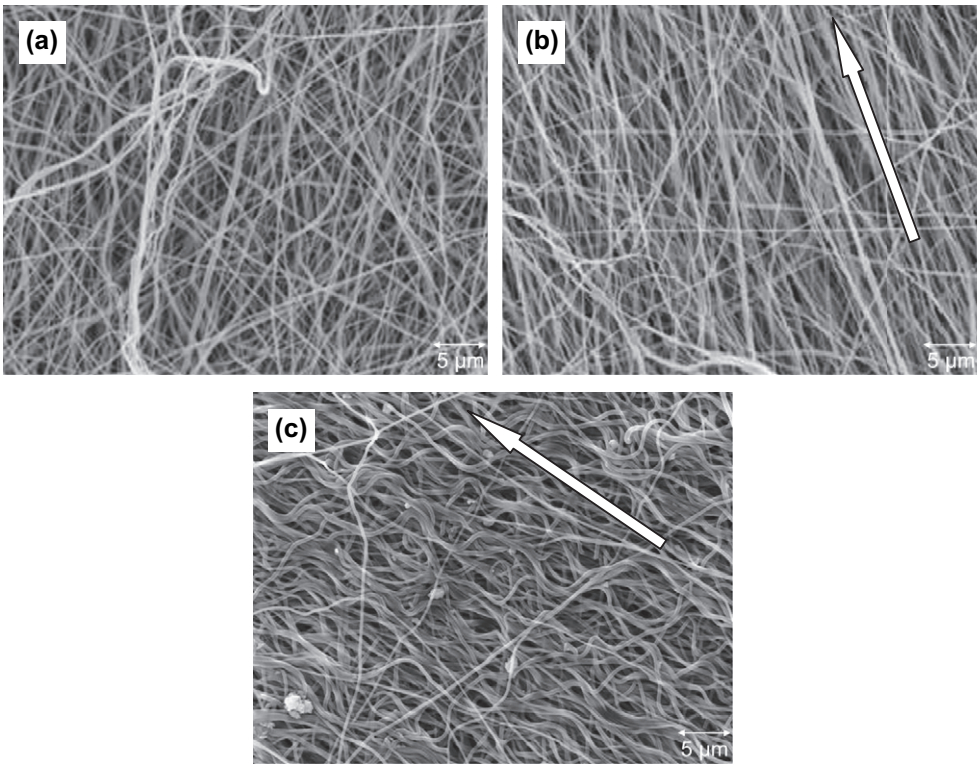

Fig. 3. SEM image of Nylon 6/0.1 wt% MWNT nanocomposite nanofibers collected at (a) 3000, (b) 4500 and (c) 6000 rpm. Arrows denote alignment direction.

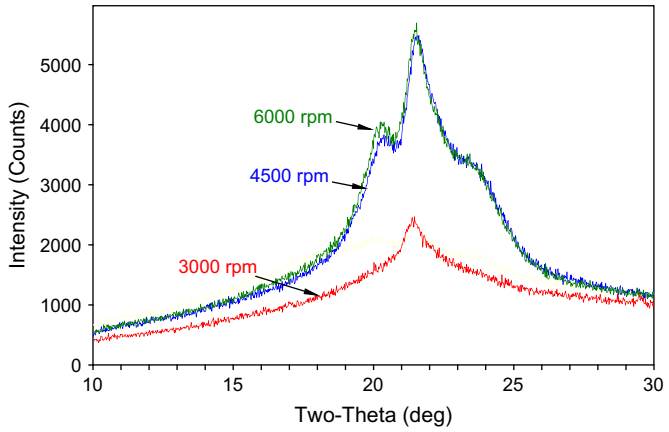

Fig. 4. XRD patterns of neat Nylon 6 fibers collected at different rotation speeds.

crystals, suggesting that electrospinning favors the less stable phase. Vasanthan and Salem [40] have studied the effect of draw ratio on Nylon 6 fibers spun from the melt, and showed that at higher draw ratios (DR = 4) the WAXD patterns showed only the presence of α crystals. Liu et al. [33] have studied the effect of nucleating agents on the modification of crystal structure of Nylon 6. It was observed that only drawing and annealing of the fibers influence the α to γ crystal transformation.

Fig. 6 shows the effect of MWNTs and take-up velocities on the melting behavior of the polymer, measured by DSC. The neat resin exhibits multiple melting endotherms, marked as $T_{m,1}$ (214 °C) and $T_{m,2}$ (223 °C), corresponding to melting of the γ and α phase crystals. The α melting peak becomes more distinctive at the highest take-up speed. A fraction of the γ phase is still present, as shown by the subtle shoulder in the DSC scan for the sample collected at 6000 rpm. This finding is different from what is observed in the XRD data, which shows a mixture of the α and γ phases. The dominance of the γ phase in the XRD scans, would be expected, since a significant level of statistical directional disorder would be expected from the e-spinning. However, the dominance of the α phase in the DSC scans may be due to melting and re-crystallization of the lower order γ phase crystals into α phase crystals during heating in the DSC. The melting temperature

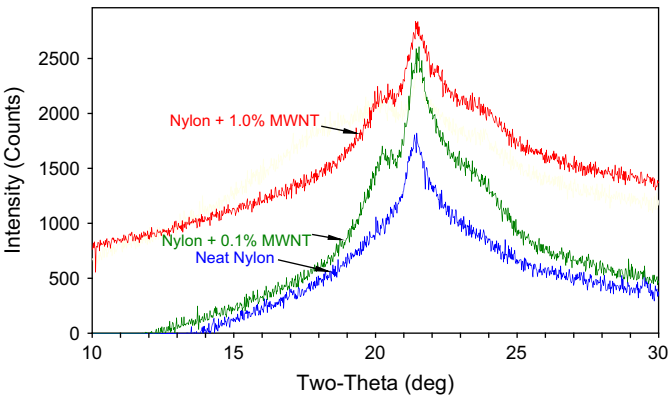

Fig. 5. XRD patterns of fibers with different nanotube loadings at 3000 rpm.

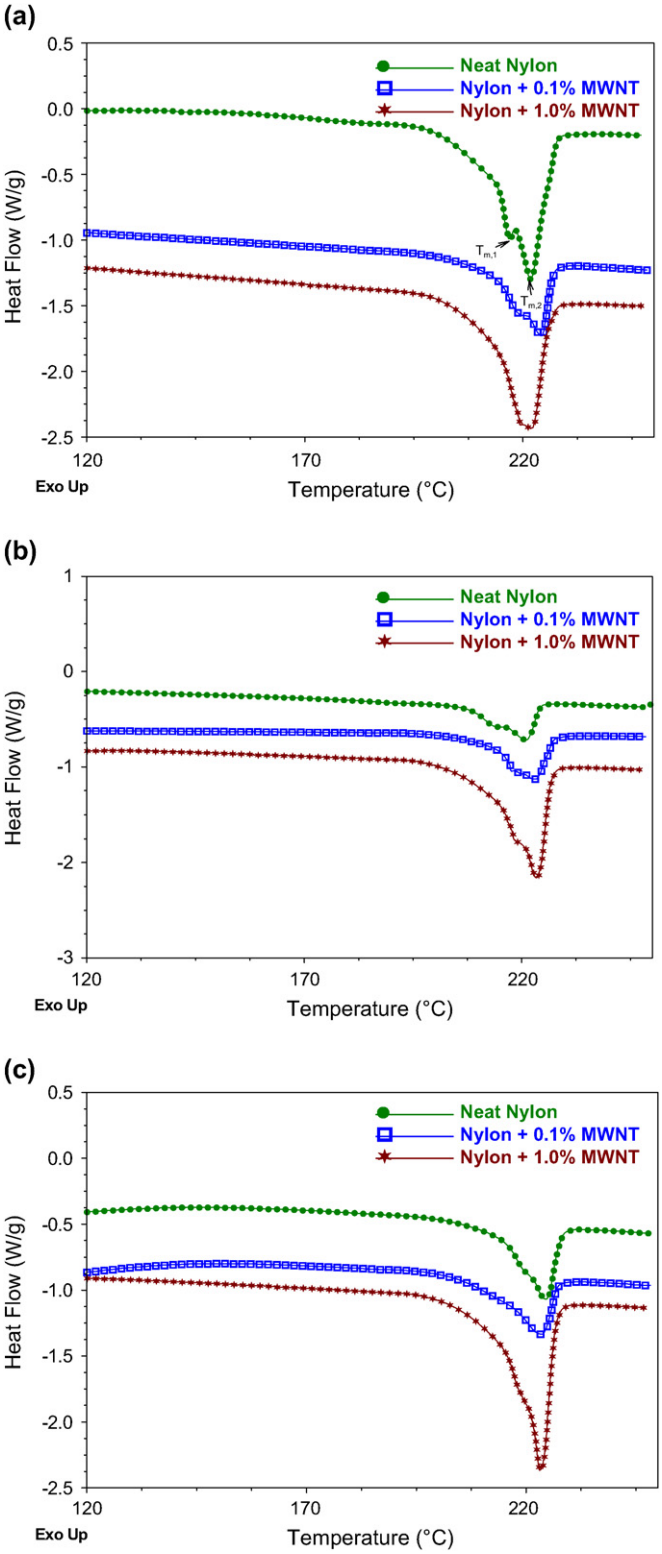

Fig. 6. DSC thermographs showing the effect of MWNT on the melting behavior of Nylon 6 at (a) 3000, (b) 4500 and (c) 6000 rpm take-up speeds.

($T_{m,2}$) and the % crystallinity variation of Nylon 6 with addition of MWNT and take-up speed are shown in Table 1. The degree of crystallinity was calculated using an enthalpy of fusion of 190 J/g for the fully crystalline material [39] and the peaks for the α and γ phases were used to compute the

Table 1
Effect of take-up speed and MWNT on the melting and crystallinity of Nylon 6

Take-up speed (rpm)	Sample	T_m (°C)	% Crystallinity
3000	Neat Nylon 6	221	43
	Nylon 6/0.1 wt% MWNT	224	36
	Nylon 6/1.0 wt% MWNT	222	32
4000	Neat Nylon 6	221	27
	Nylon 6/0.1 wt% MWNT	223	35
	Nylon 6/1.0 wt% MWNT	223	40
6000	Neat Nylon 6	224	38
	Nylon 6/0.1 wt% MWNT	223	35
	Nylon 6/1.0 wt% MWNT	223	39

enthalpy of fusion. The melting temperatures show essentially no change with increased take-up speed and nanotube loading. Morphological differences may have been erased by the annealing effect of the DSC scan, as discussed earlier. For the neat resin, the degree of crystallinity drops, then recovers as the take-up velocity increases. Although the % crystallinity recovers at the highest take-up velocity, the overall magnitude is still less than that for the lowest take-up velocity. For a given collector speed, a slight crystallinity increase with nanotube loading is observed. When similar nanotube loadings are compared, essentially no change in crystallinity with take-up speed is observed. A similar trend was observed by Liu et al. [37] for the crystallization behavior of melt compounded Nylon 6/MWNT nanocomposite. They observed that the metastable γ crystals were transformed to stable α crystals with increased annealing temperature. Similarly, Fong et al. [35] have observed the formation of γ phase in the neat Nylon 6 and Nylon 6/montmorillonite nanocomposite electrospun nanofibers. These observations suggest that metastable γ form is the preferred form of crystal structure of Nylon 6 in melt spinning as well as electrospinning.

In our study, the combination of the MWNTs, which can be considered as a nucleating agent, and the electrospinning process, resulted in a mixture of the two phases. This is in contrast to electrospun Nylon 6/silicate nanofibers, which were found to crystallize in only the γ form by Fong et al. [35]. It should be noted that since they used a manually oscillated target to collect aligned fibers, the collector speed was much lower than those used in our study. The confining effect of the two-dimensional environment of the silicates (versus the one-dimensional nature of the nanotubes) is believed to play a large role in disrupting packing of the chains into the α phase [37]. In the case of the Nylon 6/MWNTs, the rapid solvent loss prevents formation of anti-parallel packing, leading to γ phase formation. A comparison of the effect of the nanoparticle on the crystal structure of Nylon 6 can be extended to melt extrusion. The melt extruded Nylon 6/MWNT nanocomposites were shown to be composed of only the α phase crystals, while melt extruded Nylon 6/silicate nanocomposites were found to be composed of only the γ phase crystals as represented elsewhere [41].

Two-dimensional XRD scans of the neat Nylon 6 and nanocomposite fiber samples provide further insight into the effect of the processing conditions of the structure formation and degree of order. Two-dimensional XRD patterns obtained from the Nylon 6/1.0 wt% MWNT samples are shown in Fig. 7. A small degree of orientation, as denoted by non-uniformity in the diffraction rings, is observed for the lowest take-up rotation speed, and more distinct equatorial arcs are evident as the take-up speed increases. Azimuthal scans from the (200) reflection permit calculation of a Herman's orientation factor (f) for the polymer. This is based on Herman's orientation equation:

$$f = \frac{3\langle \mathrm{Cos}^2\,\varphi \rangle - 1}{2}$$

where φ defines the average angle between the molecular axis and the fiber direction [42]. Values of f for the neat Nylon 6 and nanocomposite fibers are listed in Table 2. The increasing

Table 2
Effect of take-up speed and MWNT on the orientation

Take-up speed (rpm)	Herman's orientation factor		
	Neat Nylon 6	Nylon 6/0.1 wt% MWNT	Nylon 6/1.0 wt% MWNT
3000	0.149	0.14	0.155
4500	0.172	0.23	0.18
6000	0.204	0.19	0.19

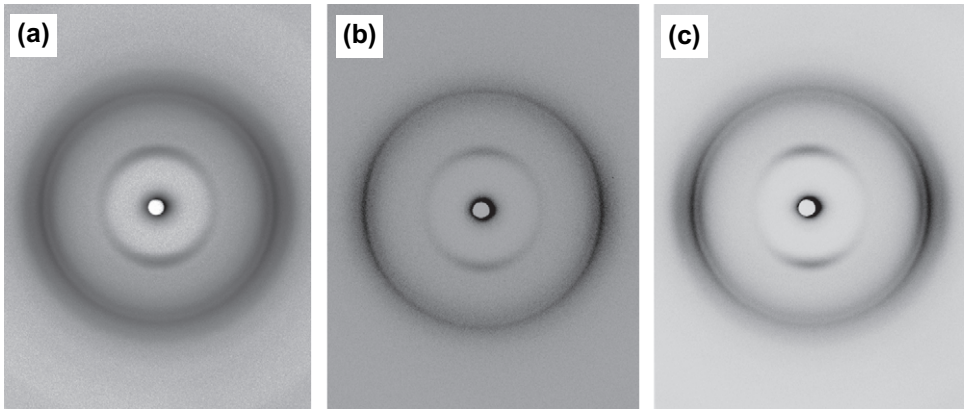

Fig. 7. Two-dimensional XRD scans for Nylon 6/1 wt% MWNT nanocomposite fibers at (a) 3000, (b) 4500 and (c) 6000 rpm.

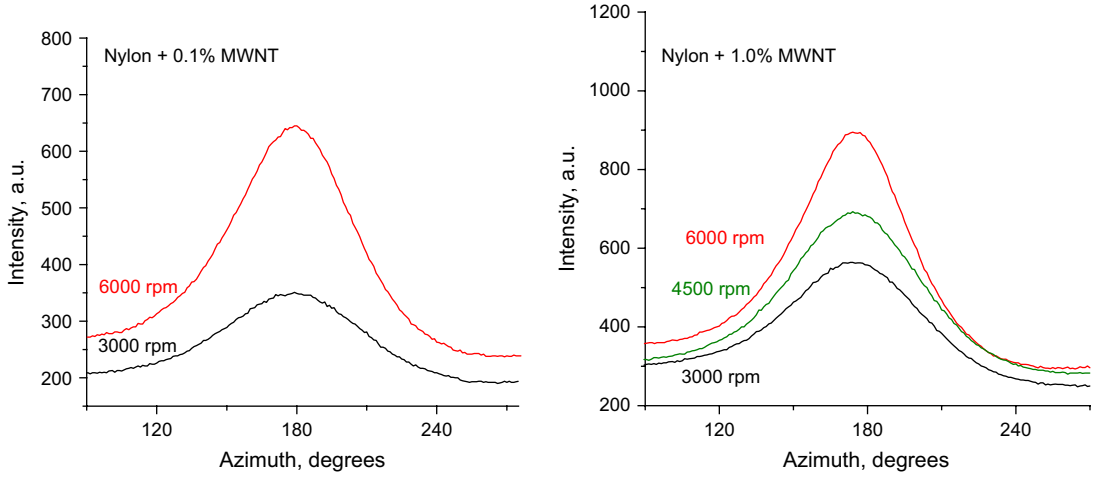

Fig. 8. Azimuthal scans of fibers with (a) Nylon 6/0.1% MWNT and (b) Nylon 6/1.0% MWNT at different take-up speeds.

values of f suggest a slight increase in molecular orientation with take-up rotation speed. The degree of orientation of neat Nylon 6 fibers is lower than the value of 0.8 as reported by Salem et al. for micron-sized Nylon 6 fibers spun using melt extrusion [29]. The high draw ratio that the jet experiences during the electrospinning process could presumably result in higher chain orientation, however, the rapid solvent evaporation is believed to inhibit development of high degrees of order. It is noteworthy that the orientation parameters as well as the degree of crystallinity of the nanocomposites (Tables 1 and 2) are higher than that obtained for the randomly aligned electrospun neat Nylon 6. This observation for the neat Nylon 6 was also reported by Fong et al. In addition to the polymer chain orientation, electrospinning can align the nanotubes, which can then serve as oriented nuclei for the polymer [26]. Herman's orientation constants can, in principle, be computed using Azimuthal scans (an example of which is shown in Fig. 8) from the (002) reflection from the MWNTs, which appears at 2θ angle of 26.5°, and corresponds to a d-spacing of 0.336 nm [26] along the fiber axis. However, this peak was not visible in the samples used in the present study, presumably due to their low concentration in the polymer matrix. Alignment of the nanotubes can be visualized in the TEM image shown below (Fig. 9) for Nylon 6/1.0 wt% MWNTs. In particular, the image in Fig. 9b shows a single, aligned nanotube embedded in the fiber. The length of the nanotube (ca. 400 nm) relative to the fiber diameter (ca. 50 nm) requires that nanotube be highly aligned. Thus the nanotubes appear to be more aligned than the Nylon 6 crystallites. This finding is similar to that reported in a related study of electrospun PAN/MWNT nanofibers, in which the nanotubes had much higher orientation constants than the polymer crystallites [26]. During electrospinning, the orientation of the small PAN crystals could relax faster than the MWNTs, and as a result, the MWNTs could retain a higher orientation than the smaller PAN crystals. In our study, a possible explanation is that due to the lack of hydrogen bond optimization during spinning, there is no mechanism for "locking in" the crystallite orientation. A similar result was obtained for the 0.1 wt% sample.

To confirm the effect of MWNTs on structural transformations, annealing was done on the fibers collected at 6000 rpm. The samples were annealed at 200 °C [40] for 1 h. Fig. 10 shows the XRD patterns obtained after annealing; clearly the fibers with a higher percentage of nanotubes attained a larger amount of α crystals, suggesting that MWNTs play a major

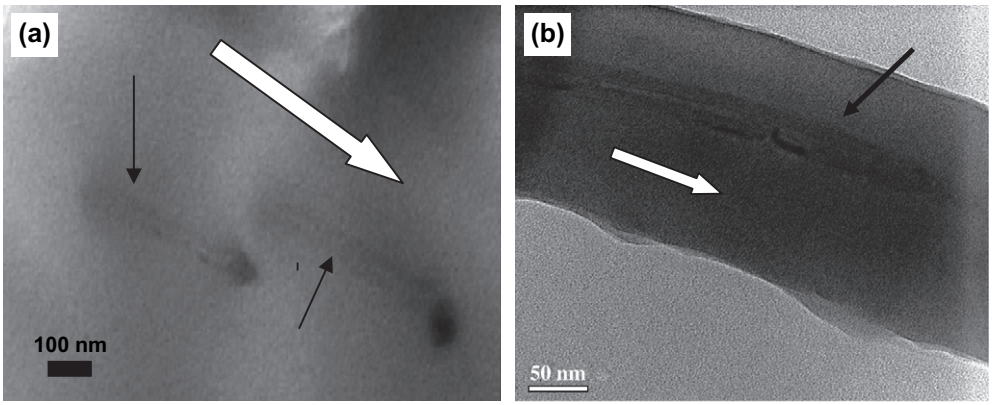

Fig. 9. TEM of 1.0 wt% carbon nanotube in Nylon 6. Black arrows denote nanotubes and white arrow denotes fiber axis.

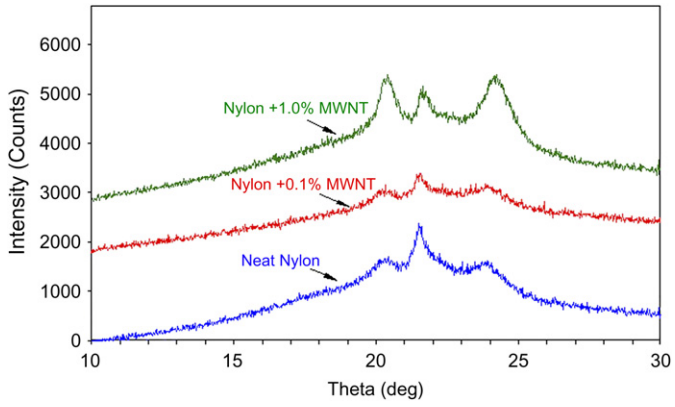

Fig. 10. XRD patterns of annealed fibers with different nanotube loadings at 6000 rpm.

role in the crystal structure transformation. This is in contrast to the observations by Liu et al. [33] which suggested that the presence of nucleating agents had no effect on the crystal structure formation.

3.3. Mechanical characterization

Dynamic mechanical analysis was conducted to study the effect of nanotube loading and collector speed on the modulus. The tensile stress was applied parallel to the orientation axis. A plot of data collected at 6000 rpm is shown in Fig. 11, and is typical of the data those were collected. The storage modulus values tabulated in Table 3 were obtained at a frequency of 10 Hz. A twofold modulus increase is observed for the neat Nylon 6 as the speed increases from 3000 to 4500 rpm, with little increase at 6000 rpm. The aligned fibers exhibited a much higher stiffness than the randomly aligned, non-woven mat. A very modest increase in modulus with nanotube loading at a given collector speed is observed, except for 6000 rpm, which exhibited a twofold modulus increase. The largest increase in modulus is observed for the 1 wt% nanotube loading at

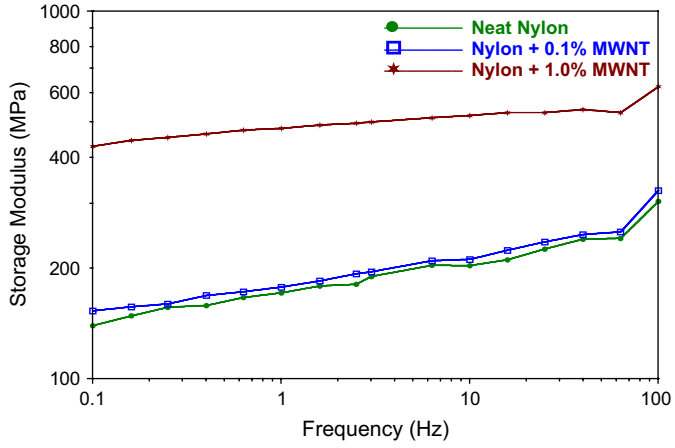

Fig. 11. Effect of MWNT on storage modulus of the non-woven aligned fiber mat at 6000 rpm.

Table 3
Storage modulus of Nylon 6 at different take-up speeds and different nanotube loadings

Take-up speed (rpm)	Sample	Storage modulus at 10 Hz (MPa)
3000	Neat Nylon 6	58
	Nylon 6/0.1 wt% MWNT	146
	Nylon 6/1.0 wt% MWNT	180
4500	Neat Nylon 6	140
	Nylon 6/0.1 wt% MWNT	147
	Nylon 6/1.0 wt% MWNT	187
6000	Neat Nylon 6	202
	Nylon 6/0.1 wt% MWNT	238
	Nylon 6/1.0 wt% MWNT	520

6000 rpm. This is expected since the enhanced drawing of the non-woven fiber will result in fiber rearrangement with the testing direction, facilitating support of the load. The effect of nanotube loading can be discerned by examining the modulus versus nanotube weight percent at a given collector speed. The most significant effect is seen at 6000 rpm, where the modulus is twice that observed at 4500 rpm. The higher property exhibited by the nanocomposite fibers correlates well with the morphological studies. First, the TEM data suggest that the nanotubes are well-dispersed and aligned in the matrix. Also, the DSC and XRD data show a transformation from the metastable γ crystal phase to α phase that contains more of the α crystals, which are known to have better mechanical properties.

4. Conclusion

Aligned nanofibrous nanocomposites of Nylon 6 and surface-modified MWNTs were successfully synthesized via electrospinning. SEM observations suggested that with increasing amounts of MWNTs the fiber diameters decreased and fiber with uniform diameter was obtained. XRD and DSC studies showed that the neat Nylon 6 transformed from a pure γ phase to a mixture of α and γ phases as the collector speed increased. For the nanocomposite, increasing the concentration of the nanotubes (without varying the take-up speed) promoted a similar transformation. The orientation of the molecular chains, as determined from Herman's orientation parameters, was relatively low, while TEM showed high nanotube alignment. We believe that during the electrospinning process, the nanotubes are oriented by the charged fluid jet, and then serve as oriented nuclei for the polymer chains. On the other hand, the lack of hydrogen bond optimization during electrospinning negates "locking in" of nylon crystallite orientation. The effect of nylon fiber alignment and enhanced carbon nanotube orientation was also manifested in mechanical properties, which increased with take-up speed and nanotube concentration. These factors (MWNTs and high take-up speed) acting concomitantly resulted in the formation of aligned nanofibrous composites with multiwalled carbon nanotube alignment and mechanical stiffness.

Acknowledgement

This work was funded by NSF DMR (Grant 0404278) and the NSF REU program.

References

[1] Iijima S. Nature 1991;354(6348):56–8.
[2] Thostenson ET, Ren Z, Chou TW. Composites Science and Technology 2001;61(13):1899–912.
[3] Collins PG, Avouris P. Scientific American 2000;283(6):62–9.
[4] Wong EW, Sheehan PE, Lieber CM. Science 1997;277(5334):1971–5.
[5] Treacy MMJ, Ebbesen TW, Gibson JM. Nature 1996;381(6584): 678–80.
[6] Feng W, Bai XD, Lian YQ, Liang J, Wang XG, Yoshino K. Carbon 2003; 41(8):1551–7.
[7] Wang XB, Liu YQ, Hu PA, Yu G, Xiao K, Zhu DB. Advanced Materials 2002;14(21):1557–60.
[8] Wei BQ, Vajtai R, Jung Y, Ward J, Zhang R, Ramanath G, et al. Nature 2002;416(6880):495–6.
[9] Thostenson ET, Chou T-W. Journal of Physics D: Applied Physics 2002; 35(16):77–80.
[10] Sennett M, Welsh E, Wright JB, Li WZ, Wen JG, Ren ZF. Applied Physics A: Materials Science and Processing 2003;76(1):111–3.
[11] Kimura T, Ago H, Tobita M, Ohshima S, Kyotani M, Yumura M. Advanced Materials 2002;14(19):1380–3.
[12] Takahashi T, Yonetake K, Koyama K, Kikuchi T. Macromolecular Rapid Communications 2003;24(13):763–7.
[13] Martin CA, Sandler JKW, Windle AH, Schwarz M-K, Bauhofer W, Schulte K, et al. Polymer 2005;46(3):877–86.
[14] Formhals A. U.S. Patent 1,975,504; 1934.
[15] Reneker DH, Chun I. Nanotechnology 1996;7(3):216–23.
[16] Seoul C, Kim Y-T, Baek C-K. Journal of Polymer Science, Part B: Polymer Physics 2003;41(13):1572–7.
[17] Salalha W, Dror Y, Khalfin RL, Cohen Y, Yarin AL, Zussman E. Langmuir 2004;20(22):9852–5.
[18] Xie X-L, Mai Y-W, Zhou X-P. Materials Science and Engineering R: Reports 2005;49(4):23.
[19] Doshi J, Reneker DH. Journal of Electrostatics 1995;35(2–3):151–60.
[20] Yarin AL, Koombhongse S, Reneker DH. Journal of Applied Physics 2001;89(5):3018–26.
[21] Huang Z-M, Zhang Y-Z, Kotaki M, Ramakrishna S. Composites Science and Technology 2003;63(15):2223–53.
[22] Dror Y, Salalha W, Khalfin RL, Cohen Y, Yarin AL, Zussman E. Langmuir 2003;19(17):7012–20.
[23] Sung JH, Kim HS, Jin H-J, Choi HJ, Chin I-J. Macromolecules 2004; 37(26):9899–902.
[24] Sundaray B, Subramanian V, Natarajan TS, Krishnamurthy K. Applied Physics Letters 2006;88(14):143114.
[25] Ge JJ, Hou H, Li Q, Graham MJ, Greiner A, Reneker DH, et al. Journal of the American Chemical Society 2004;126(48):15754–61.
[26] Hou H, Ge JJ, Zeng J, Li Q, Reneker DH, Greiner A, et al. Chemistry of Materials 2005;17(5):967–73.
[27] Ko F, Gogotsi Y, Ali A, Naguib N, Ye H, Yang G, et al. Advanced Materials 2003;15(14):1161–5.
[28] Sen R, Zhao B, Perea D, Itkis ME, Hu H, Love J, et al. Nano Letters 2004;4(3):459–64.
[29] Salem D, Moore R, Weigmann H. Journal of Polymer Science, Part B: Polymer Physics 1987;25:567–89.
[30] Bankar VG, Spruiell JE, White JL. Journal of Applied Polymer Science 1977;21(9):2341–58.
[31] Gogolewski S, Pennings AJ. Polymer 1985;26(9):1394–400.
[32] Hancock TA, Spruiell JE, White JL. Journal of Applied Polymer Science 1977;21(5):1227–47.
[33] Liu T, Dersch R, Schaper AK, Greiner A, Wendorff JH. Journal of Polymer Science, Part A: Polymer Chemistry 2003;41(4):545–53.
[34] Fan G, Zhu L, Hedin N, Fong H. Polymeric Materials: Science and Engineering 2005;93(2):482–4.
[35] Fong H, Liu W, Wang C-S, Vaia RA. Polymer 2002;43(3):775–80.
[36] Eitan A, Jiang K, Dukes D, Andrews R, Schadler LS. Chemistry of Materials 2003;15(16):3198–201.
[37] Liu T, Phang IY, Shen L, Chow SY, Zhang W-D. Macromolecules 2004; 37(19):7214–22.
[38] Clark ES. International Symposium on Intra- and Intermolecular Forces, The International Union of Crystallography, The Pennsylvania State University, August 13–17, 1974.
[39] Inoue M. Journal of Polymer Science, Part A: General Papers 1963;1(8): 2697–709.
[40] Vasanthan N, Salem DR. Journal of Polymer Science, Part B: Polymer Physics 2001;39(5):536–47.
[41] Lincoln DM, Vaia RA, Wang Z-G, Hsiao BS. Polymer 2001;42(4): 1621–31.
[42] Samuels RJ. Structured polymer properties. New York: Wiley-Interscience; 1974.